Polarization manipulation of surface acoustic waves by metallization patterns on a piezoelectric substrate

R. Weser, A. N. Darinskii, and H. Schmidt

View Online   Export Citation   CrossMark

ARTICLES YOU MAY BE INTERESTED IN

Polarization manipulation of surface acoustic waves by metallization patterns on a piezoelectric substrate

View Online   Export Citation   CrossMark

R. Weser,[1,a] (iD) A. N. Darinskii,[2] and H. Schmidt[1]

AFFILIATIONS

[1] Leibniz Institute for Solid State and Materials Research Dresden (IFW Dresden), SAWLab Saxony, Helmholtzstr. 20, 01069 Dresden, Germany

[2] Institute of Crystallography FSRC "Crystallography and Photonics," Russian Academy of Sciences, Leninskii pr. 59, Moscow 119333, Russia

[a] Author to whom correspondence should be addressed: r.weser@ifw-dresden.de

ABSTRACT

Surface acoustic waves (SAWs) with large normal (vertical) surface displacement at the surface are commonly utilized in microfluidic actuators in order to provide the desired momentum transfer to the fluid. We present an alternative concept using a SAW with comparatively small vertical displacement. Such a SAW passes underneath the microfluidic vessel walls with minimum losses but it needs to be converted inside the vessel into surface vibrations with large vertical displacements. The principal operability of the above idea is illustrated by experimental and numerical studies of the polarization conversion of a leaky SAW on 64° rotated Y-cut of lithium niobate owing to the partial metallization of the substrate surface. In particular, it is found that vertical displacements on the metallized surface can be up to 3.5 times higher as compared to their values on the free surface. Results of computations agree reasonably well with measurements carried out with a laser Doppler vibrometer and allow the clarification of some specific features of this polarization conversion by means of spatial frequency analysis.

Surface acoustic waves (SAWs) are utilized in various devices, including frequency filters,[1–3] sensors,[4–9] and actuators.[10–21] Besides the spatial distribution of mechanical displacement components, the polarization at the surface is another characteristic feature for the application of SAW. The polarization of SAW does not play a significant role for SAW devices such as frequency filters and gas sensors, whereas it is crucial for fluid sensors and, in particular, for actuators. In fluid sensors, most often SAWs with dominating horizontal, i.e., parallel to the substrate boundary, displacement are employed due to their high sensitivity against fluidic surface loading while undergoing acceptable attenuation.[7–9]

In contrast, actuators mainly deploy SAW with large surface normal, i.e., vertical, displacement in order to ensure the transfer of momentum between the substrate surface and the fluid (e.g., see Refs. 22 and 23). Below, we conventionally call the two types of SAW as horizontally polarized (HP) and vertically polarized (VP). Note that even HP SAWs have been demonstrated to drive microfluidic streaming and atomization.[24,25] However, SAW-based microfluidic actuators,

used to induce fluid motion or to manipulate immersed particles and cells, mainly utilize Rayleigh SAW characterized by a large vertical displacement amplitude.[10–21] The presence of microfluidic vessels needed to confine the fluid causes additional attenuation of the incident Rayleigh SAW and, thus, worsens the overall device performance[26] while also causing damages of the vessel wall during power operation.

To overcome this drawback, one can generate a HP SAW that transmits the vessel wall with less attenuation compared to a VP SAW.[27] Inside the fluidic vessel, the HP SAW subsequently needs to be converted to increase the normal surface displacement amplitude in order to ensure efficient microfluidic actuation. This polarization conversion can be achieved by an abrupt change of the mechanical and/or the electrical boundary conditions for SAW propagation. Note that the SAW polarization conversion has been demonstrated for phononic waveguides to generate non-piezoelectric wave modes.[28]

In the present paper, we experimentally and theoretically investigate the SAW polarization conversion induced by thin film metallization patterns deposited on the working surface of a piezoelectric

TABLE I. Characteristic data of SAW modes on 64°YX-LiNbO$_3$: complex phase velocity and amplitude of unit polarization vector components (material constants are taken from[29]).

Wave	Velocity (m/s)	Components of polarization vector at the surface		
64YX-LSAW	4692–4.5i	$\|A_{f,x}\| = 0.27$	$\|A_{f,y}\| = 0.95$	$\|A_{f,z}\| = 0.16$
64YX-LSAWm	4445–0.25i	$\|A_{m,x}\| = 0.11$	$\|A_{m,y}\| = 0.93$	$\|A_{m,z}\| = 0.35$
64YX-SAW	3680	$\|A_{sx}\| = 0.23$	$\|A_{s,y}\| = 0.56$	$\|A_{s,z}\| = 0.79$

substrate. Namely, we study the selective manipulation of boundary conditions for the leaky SAW propagating parallel to the crystal's X-axis on 64° Y-rotated lithium niobate (LiNbO$_3$) cut (64YX-LSAW). This wave is predominantly shear-horizontally polarized (Table I). It is well-known that mechanical strains inside the substrate can induce electric fields in the adjoining medium via the piezoelectric effect, so the velocity and the polarization vector of SAW depend on the electric boundary conditions.[1–3] Based on this fact, we have investigated the polarization conversion due to a metal thin film that locally changes the electric boundary condition, causing the electric potential to vanish above the substrate.

The SAW devices used for experimental investigations consist of a single crystal LiNbO$_3$ substrate (64° rotated Y-cut with X-propagation direction: 64°YX LiNbO$_3$, thickness 510 μm) and a thin film metallization. The LSAW is generated by an interdigital transducer (IDT). Two types of conventional solid electrodes, i.e., λ/4 IDTs (metallization ratio: 0.5), are used with the same aperture w = 2 mm but different periods: $\lambda = 30\,\mu$m and $\lambda = 120\,\mu$m. The number of electrode pairs is chosen to be N = 14 and N = 22, respectively, yielding an electrical impedance of the IDT well-matched to 50 Ω. The polarization conversion is induced by a metallized area arranged at a distance of 1 mm ($\lambda = 30\,\mu$m) and 3 mm ($\lambda = 120\,\mu$m) with respect to the front of the IDT. The area between the IDT and the metallization pattern is free substrate surface. Three different configurations are investigated: (1) the free substrate surface without any metallization, (2) a continuous metallization, and (3) metal strips of width 5λ periodically arranged with a period of 10λ parallel to the IDT electrodes (Fig. 1).

The dimension of the metallization pattern perpendicular to the SAW propagation direction is chosen to comprise the full substrate width and, therefore, is even larger with respect to the IDT aperture. IDT and metallization pattern on all samples are fabricated via

electron-beam evaporation and lift-off technique of subsequent titanium and aluminum layers of thickness 5 nm and 295 nm, respectively. Besides the primary fabrication procedures, the SAW devices need an additional preparation in order to suppress bulk and surface wave reflections. To do so, a waffle-weave pattern is diced into the back side of the substrate and the substrate edges parallel to the IDT electrodes are beveled and covered with highly viscous photo resist.[30] The SAW devices are mounted on a custom chip holder and electrically connected using printed circuit boards comprising coplanar waveguides matched to a 50 Ω characteristic impedance and gold-plated spring pins. Characterization of the electrical behavior is carried out via electrical S-parameter measurements with a vector network analyzer (VNA, Agilent E5071C). The lateral distribution of normal surface displacement u$_z$ in terms of amplitude and phase is measured with a scanning laser Doppler vibrometer (LDV, Polytec UHF 120).

The frequency dependent reflection coefficient $|S_{11}|$ provided by electrical characterization exhibits the typical behavior with a minimum due to the resonant properties of the IDT (not shown here; see Ref. 31 for details). The $|S_{11}|$ minimum frequency is approximately 37 MHz ($\lambda = 120\,\mu$m) and 148 MHz ($\lambda = 30\,\mu$m). Based on the electrical characterization, we have already demonstrated that the photo resist in combination with the back side treatment can suppress undesired reflections of LSAW and of bulk acoustic waves (BAW). However, electrical measurements with only one IDT do not allow for a complete characterization of acoustic wave propagation, including reflections, because reflected waves can only be detected if they return to the single IDT appropriately.

Measuring the normal surface component u$_z$ of displacements at the working surface provides a deeper insight into the distribution of the wave field and the role of a waffle-weave pattern diced on the substrate back side. Initially, LDV measurements are carried out for a SAW device with an IDT period $\lambda = 120\,\mu$m and free surface before and after back side treatment. Direct comparison of experimental results (see Fig. S1 in the supplementary material), as well as significantly better agreement with simulation results (Figs. 2 and 4), indicate that the back side treatment is capable of efficiently suppressing BAW interference at the surface (details of the computational method are outlined in the supplementary material; see also Refs. 27 and 30–37).

Figure 2 shows the results of experiment and simulation for SAW devices with $\lambda = 120\,\mu$m with and without metallization pattern. The electrical voltage applied to the IDT during LDV measurements is determined and subsequently used for computations of displacement amplitude, yielding a reasonably good qualitative and quantitative agreement between experiment and simulation. Thus, the model is capable of adequately accounting for the electroacoustic transmission behavior of the IDT–substrate combination, as well as for the presence of a surface metallization in front of the IDT. For free surface (no
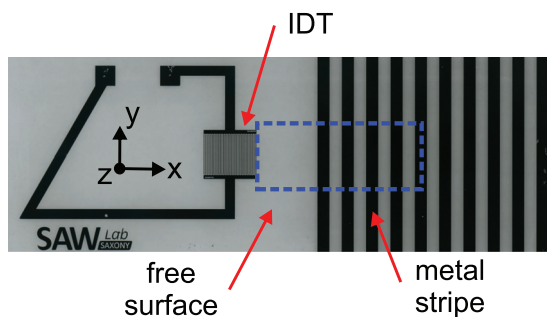
FIG. 1. Photograph of the SAW device with the interdigital transducer (IDT) and periodically arranged strips of metallization. SAW propagation direction is parallel to the x-axis, LDV scan area is marked in blue.
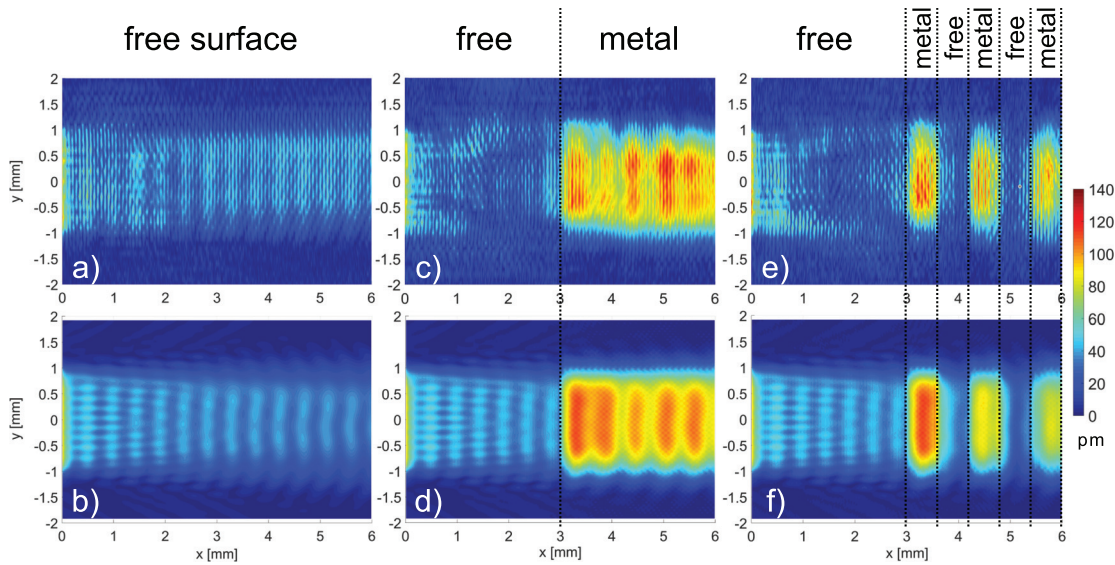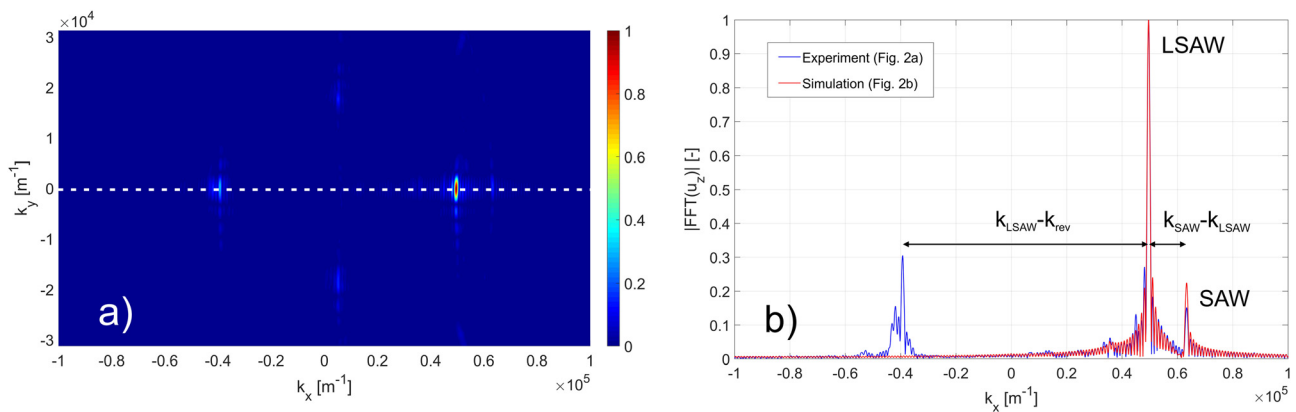
FIG. 2. Normal surface displacement amplitude $|u_z|$ for SAW devices with IDT period $\lambda = 120\,\mu m$ evaluated at 37 MHz: (a) and (b) free surface; (c) and (d) continuous metallization; (e) and (f) metal strips and (a), (c), and (e) LDV measurement; and (b), (d), and (f) simulation. An equivalent voltage was applied to all samples for both experiment and simulation.

metallization), a rather small amplitude $|u_z|$ can be observed from experiment [Fig. 2(a)] and simulation [Fig. 2(b)] due to the dominant horizontal polarization of the LSAW excited by the IDT. However, the SAW beam can be clearly identified for $|y| \leq 1\,mm$ due to the limited IDT aperture.

Since LDV measurements provide both the amplitude and the phase of the normal surface displacement, the discrete two-dimensional Fourier transformation can be applied to decompose the wave field at the substrate surface in order to identify existing principal waves by their characteristic wave vector components $K = (k_x, k_y)$. Figure 3(a) depicts the spatial frequency domain representation of LDV measurement data for the SAW device with a $120\,\mu m$ IDT

period and free surface [cf. Fig. 2(a)]. The overall maximum appears for $K_{LSAW} = (k_x = 49632\ m^{-1},\ k_y = 0)$, indicating the 64YX-LSAW propagating parallel to the x-axis with wavelength $\lambda_{LSAW} = 126.6\,\mu m$, which is very close to the theoretical value $126.8\,\mu m$ (as derived from the real part of the phase velocity given in Table I and frequency 37 MHz). The superposition of this wave with the 64YX-SAW ($K_{SAW} = (k_x = 63\,349\ m^{-1},\ k_y = 0)$, $\lambda_{SAW} = 99.2\,\mu m$) yields an amplitude modulation in the spatial domain with a period of $458\,\mu m$ [cf. Figs. 2(a) and 2(b)] originating from the difference in wave numbers [$K_{SAW} - K_{LSAW} = 13717\ m^{-1}$, Fig. 3(b)]. The 64YX-SAW exists on the same cut (Table I) and is generated in parallel with 64YX-LSAW, probably because of multiple reflections inside the IDT since the

FIG. 3. Spatial frequency domain representation of the normal surface displacement amplitude u_z for the SAW device with IDT period $\lambda = 120\,\mu m$ and free surface (cf. Figs. 2(a) and 2(b)) evaluated at 37 MHz: (a) 2D Fourier spectrum as a function of wave numbers k_x and k_y. Complex LDV data are evaluated for $-2\,mm < y \leq 2\,mm$ and $0 < x \leq 6\,mm$ using the 2D FFT algorithm. Absolute value of Fourier transform is scaled to the maximum; (b) cross section of 2D Fourier spectrum for $k_y = 0$ (dashed white line in (a) of measured (blue) and simulated (red) displacement amplitude u_z.

64YX-SAW is practically non-piezoactive. Note that, although the z-displacement of 64YX-SAW is around 15% [Fig. 3(b), blue line] that of 64YX-LSAW, the total amplitude of 64YX-SAW does not exceed 3% of 64YX-LSAW since $|A_{s,z}|/|A_{f,z}| = 5$ (Table I).

Additional peaks can be observed for $|k_y| \approx 18\,000$ m^{-1}, i.e., $k_x = 4800$ m^{-1}, indicating standing wave components caused by reflections of bulk waves from the waffle-weave pattern at the backside of the substrate also yielding waves propagating in the y-direction ($k_y \neq 0$). There is another maximum at $k_{rev} = -40\,000$ m^{-1}, which is clearly seen only from the experimental data [Fig. 3(b), blue line]. It seems reasonable to believe that this peak corresponds to reflected wave components propagating in the reverse direction, in particular, because it is not seen from simulation data where PML prevents any kind of reflections at the substrate backside and edges. Since we cannot identify according modes around $+k_{rev}$, they are probably bulk wave components reversely reflected by the periodic relief of the backside of the substrate. At the same time, we believe that it is these modes with wavenumbers around k_{rev} that interfere with 64YX-LSAW on the free surface and with 64YX-LSAWm on the metallized area, causing, thereby, strong ripples of $|u_z(x)|$ with a period of about 70 μm (see also Fig. S2 in the supplementary material). These ripples can also be observed from experimental data in Fig. 2.

In the presence of a continuous metallization [Figs. 2(c) and 2(d)], surface normal amplitude strongly increases within a distance of about 2–3 wavelengths after the LSAW passes the transition from free to metallized surface. The LSAW on the metallized surface (64YX-LSAWm) shows different characteristics compared to those of 64YX-LSAW (Table I). Importantly, the z-displacement amplitude increases by the factor $|A_{m,z}|/|A_{f,z}| = 2.2$, although the y-displacement of both waves is the greatest one. Additionally, the energy flux of 64-YX LSAW is 1.58 times that of 64-YX LSAWm for equal amplitudes as given by the unit polarization vector at the surface (Table I). This difference is basically due to markedly different penetration depths of both waves basically stipulated by the difference in the real part of phase velocities.

Assuming an ideal transfer of energy from LSAW to LSAWm and considering the overall increase in the normal surface displacement amplitude caused by polarization conversion of LSAW into LSAWm, the according amplitude ratio is given by $2.2 \cdot \sqrt{1.58} = 2.75$. Frequency domain evaluation of experimental data [Figs. 2(a) and 2(c)] allows for the determination of the z-displacement amplitude of LSAWm and LSAW due to their different wave vector components (see the supplementary material, Fig. S3), yielding an amplitude ratio $|u_{m,z}|/|u_{f,z}| = 2.6$, which is in reasonably good agreement with the theoretical value. Additionally, the constructive interference of 64YX-LSAWm with, e.g., the non-piezoactive 64YX-SAW, further raises the local normal surface displacement amplitude by 30%, yielding a periodical increase by the factor of 3.5 as compared to the original 64YX-LSAW (see also Fig. S2 in the supplementary material).

In the case of periodic metal strips [Figs. 2(e) and 2(f)], the amplitude increases at transitions from free to metallized surface and decreases at transitions from metallized to free surface, both within a propagation distance of about 2–3 wavelengths. According to estimations based on the lateral amplitude $|u_z(x,y)|$, the z-displacement on the first strip in average is 3.5 times the z-displacement in the incident LSAW, which seems reasonable compared to continuous metallization (applying the Fourier analysis is impossible because the strip width is

only 5λ). Maximum values diminish with each further strip. This effect can be seen more clearly from the results of the SAW device with an IDT period $\lambda = 30$ μm and periodic metal strips (Fig. 4) due to the larger number of involved metal strips. A considerable decrease in amplitude from strip to strip can be ascribed to the radiation into the bulk of the substrate, which occurs to be stronger between strips than just on the free surface far enough from any obstacles, since the gap is only 5λ wide and the wave field within it has no opportunity to transform to 64YX-LSAW.

In summary, we have experimentally and numerically investigated the polarization conversion of a leaky SAW (LSAW) on 64°YX LiNbO$_3$ substrate induced by a metal thin film. The LSAW on both free and metallized surfaces is shear-horizontally polarized with a dominant in-plane component of mechanical displacement perpendicular to the propagation direction. However, in the presence of a metal film on the surface, the boundary conditions of SAW propagation abruptly change with respect to the free surface and the polarization is manipulated yielding an increase in normal surface displacements by a factor of 2.6. Computations reveal that this effect basically emerges due to the change in electrical boundary conditions induced by the metal film, which fully screens the piezoelectric substrate, so that the electric field accompanying the LSAW no longer penetrates outside the substrate and, thus, the characteristics of the wave change. The mechanical loading brought in by the Al film plays a negligible role in the cases under consideration. The abruptly changing boundary conditions of LSAW propagation lead to a change of polarization, i.e., in this case, a significant increase in surface normal mechanical displacement u_z. Constructive interference with other waves, in particular, with the non-leaky SAW, causes an additional localized increase in u_z, characterized by a spatial modulation period due to the different wave vectors of LSAW and SAW, yielding a total amplitude factor of 3.5.

Our concept of SAW polarization conversion demonstrated here is of particular interest for different applications in SAW-driven microfluidics due to the fact that the SAW polarization can be selectively manipulated simply by tailoring the lateral layout of the metallization pattern. Once a HP SAW is excited anywhere outside the fluidic region, its normal surface displacement amplitude can be increased inside the vessel while the SAW propagates along the substrate–fluid interface. The presented approach provides two key advantages for SAW-driven microfluidics: The attenuation of HP SAW during the transmission of vessel walls is significantly reduced and the lateral position of momentum transfer, i.e., the radiation of
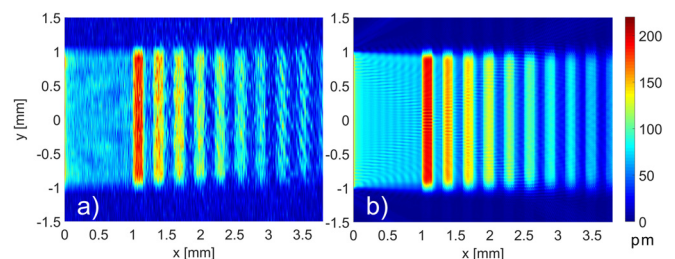
FIG. 4. Normal surface displacement amplitude $|u_z|$ for the SAW device with periodic strip metallization and IDT period $\lambda = 30$ μm evaluated at 148 MHz: (a) LDV measurement and (b) simulation. An equivalent voltage was applied to the IDT for both experiment and simulation.

bulk waves into the fluid, and so the location of SAW-based manipulation, inside the microfluidic vessel can be easily and precisely defined by means of layout.

See the supplementary material for details on the influence of the substrate backside treatment, the computational method, and the determination of the leaky SAW amplitudes in free and metallized areas.

DATA AVAILABILITY

The data that support the findings of this study are available within the article and its supplementary material.

REFERENCES

[1]C. K. Campbell, *Surface Acoustic Wave Devices* (Academic Press, 1998).

[2]K. Hashimoto, *Surface Acoustic Wave Devices in Telecommunications* (Springer-Verlag, Berlin, 2000).

[3]D. Morgan, *Surface Acoustic Wave Filters* (Elsevier, 2007).

[4]S. Shiokawa and J. Kondoh, "Surface acoustic wave sensors," Jpn. J. Appl. Phys., Part 1 **43**(5B), 2799–2802 (2004).

[5]J. Devkota, P. R. Ohodnicki, and D. W. Greve, "SAW sensors for chemical vapors and gases," Sensors **17**(4), 801 (2017).

[6]K. Länge, "Bulk and surface acoustic wave sensor arrays for multi-analyte detection: A review," Sensors **19**, 5382 (2019).

[7]J. Kondoh, "Liquid-phase sensor using shear horizontal surface acoustic wave devices," IEEJ Trans. Electron. Inf. Syst. **131**(2), 1094–1100 (2011).

[8]F. Josse, F. Bender, and R. W. Cernosek, "Guided shear horizontal surface acoustic wave sensors for chemical and biochemical detection in liquids," Anal. Chem **73**, 5937–5944 (2001).

[9]F. Martin, M. I. Newton, G. McHale, K. A. Melzak, and E. Gizeli, "Pulse mode shear horizontal-surface acoustic wave (SH-SAW) system for liquid based sensing applications," Biosens. Bioelectron. **19**, 627–632 (2004).

[10]T. Franke, A. R. Abate, D. A. Weitz, and A. Wixforth, "Surface acoustic wave (SAW) directed droplet flow in microfluidics for PDMS devices," Lab Chip **9**, 2625–2627 (2009).

[11]L. Y. Yeo and J. R. Friend, "Surface acoustic wave microfluidics," Ann. Rev. Fluid Mech. **46**, 379 (2014).

[12]X. Ding, P. Li, S.-C. Steven Lin, Z. S. Stratton, N. Nama, F. Guo, D. Slotcavage, X. Mao, J. Shi, F. Costanzo, and T. J. Huang, "Surface acoustic wave microfluidics," Lab Chip **13**, 3626–3649 (2013).

[13]W. Connacher, N. Zhang, A. Huang, J. Mei, S. Zhang, T. Gopesh, and J. Friend, "Micro/nano acoustofluidics: Materials, phenomena, design, devices, and applications," Lab Chip **18**, 1952 (2018).

[14]M. Sesen, T. Alan, and A. Neild, "Microfluidic on-demand droplet merging using surface acoustic waves," Lab. Chip **14**, 3325 (2014).

[15]D. J. Collins, O. Manor, A. Winkler, H. Schmidt, J. R. Friend, and L. Y. Yeo, "Atomization off thin water films generated by high-frequency substrate wave vibrations," Phys. Rev. E **86**, 056312 (2012).

[16]A. Winkler, S. M. Harazim, S. B. Menzel, and H. Schmidt, "SAW-based fluid atomization using mass-producible chip devices," Lab Chip **15**, 3793–3799 (2015).

[17]A. Winkler, S. Harazim, D. J. Collins, R. Brünig, H. Schmidt, and S. Menzel, "Compact SAW aerosol generator," Biomed. Microdevices **19**, 9 (2017).

[18]F. Kiebert, S. Wege, J. Massing, J. Lönig, C. Cierpka, R. Weser, and H. Schmidt, "3D measurement and simulation of surface acoustic wave driven fluid motion: A comparison," Lab. Chip **17**, 2104 (2017).

[19]D. J. Collins, B. L. Khoo, Z. Ma, A. Winkler, R. Weser, H. Schmidt, J. Hanbde, and Y. Ai, "Selective particle and cell capture in a continuous flow using micro-vortex acoustic streaming," Lab Chip **17**, 1769–1777 (2017).

[20]A. Fakhfouri, C. Devendran, T. Albrecht, D. J. Collins, A. Winkler, H. Schmidt, and A. Neild, "Surface acoustic wave diffraction driven mechanisms in microfluidic systems," Lab Chip **18**, 2214–2224 (2018).

[21]R. Weser, A. Winkler, M. Weihnacht, S. Menzel, and H. Schmidt, "The complexity of surface acoustic wave fields used for microfluidic applications," Ultrasonics **106**, 106160 (2020).

[22]A. D. Pierce, *Acoustics* (Acoustical Society of America, Woodbury, 1991).

[23]L. D. Landau and E. M. Lifshitz, *Fluid Mechanics*, 2nd ed. (Pergamon Press, Oxford, 1993).

[24]D. S. Brodie, Y. Q. Fu, Y. Li, M. Alghane, R. L. Reuben, and A. J. Walton, "Shear horizontal surface acoustic wave induced microfluidic flow," Appl. Phys. Lett. **99**, 153704 (2011).

[25]H.-F. Pang, K.-M. Fan, Y.-Q. Fu, F. Placido, J.-Y. Ma, and X.-T. Zu, "Droplet streaming and nebulization induced by the shear horizontal surface acoustic wave," Adv. Mater. Res. **662**, 580–585 (2013).

[26]A. Winkler, R. Brünig, C. Faust, R. Weser, and H. Schmidt, "Towards efficient surface acoustic wave (SAW)-based microfluidic actuators," Sens. Actuators, A **247**, 259–268 (2016).

[27]A. N. Darinskii, M. Weihnacht, and H. Schmidt, "Acoustomicrofluidic application of quasi-shear surface waves," Ultrasonics **78**, 10 (2017).

[28]Z. Shen, W. Fu, R. Cheng, H. Townley, C.-L. Zou, and H. X. Tang, "Polarization mode hybridization and conversion in phononic wire waveguides," Appl. Phys. Lett. **115**, 201901 (2019).

[29]G. Kovacs, M. Anhorn, H. E. Engan, G. Visintini, and C. C. W. Ruppel, "Improved material constants for LiNbO₃ and LiTaO₃," in Proceedings of the IEEE Ultrasonics Symposium (1990), pp. 435–438.

[30]A. N. Darinskii, M. Weihnacht, and H. Schmidt, "Computation of the pressure field generated by surface acoustic waves in microchannels," Lab Chip **16**, 2701–2709 (2016).

[31]R. Weser, A. Darinskii, and H. Schmidt, "Polarization conversion of surface acoustic waves for enhanced microscale actuation applications," in IEEE International Ultrasonics Symposium (IUS), Glasgow, UK (2019), pp. 683–686.

[32]A. N. Darinskii, M. Weihnacht, and H. Schmidt, "Surface acoustic wave scattering from steps, grooves, and strips on piezoelectric substrates," IEEE Trans. Ultrason., Ferroelectr., Freq. Control **57**(9), 2042–2050 (2010).

[33]A. N. Darinskii, M. Weihnacht, and H. Schmidt, "Usage of symmetry in the simulation of interdigital transducers," IEEE Trans. Ultrason., Ferroelectr., Freq. Control **57**(10), 2356–2359 (2010).

[34]A. N. Darinskii, M. Weihnacht, and H. Schmidt, "Mutual conversion of bulk and surface acoustic waves in gratings of finite length on half-infinite substrates. I. FE analysis of surface wave," Ultrasonics **53**(5), 998–1003 (2013).

[35]A. N. Darinskii, M. Weihnacht, and H. Schmidt, "Mutual conversion of bulk and surface acoustic waves in gratings of finite length on half-infinite substrates. II. FE analysis of bulk wave generation," Ultrasonics **53**(5), 1004–1011 (2013).

[36]A. N. Darinskii, M. Weihnacht, and H. Schmidt, "Surface acoustic wave reflection/transmission at vertical borders of piezoelectric substrates," Ultrasonics **56**, 318–324 (2015).

[37]R. Weser, A. N. Darinskii, M. Weihnacht, and H. Schmidt, "Experimental and numerical investigations of mechanical displacements in surface acoustic wave bounded beams," Ultrasonics **106**, 106077 (2020).